bioRxiv preprint doi: https://doi.org/10.1101/219931; this version posted November 15, 2017. The copyright holder for this preprint (which was not certified by peer review) is the author/funder. All rights reserved. No reuse allowed without permission.

Multiple spin echos in cerebral dynamics: Evidence for spontaneous symmetry breaking during pulsation

Christian Kerskens*
Trinity College Institute of Neuroscience, Trinity College Dublin, Dublin, Ireland

David López Pérez
Neurocognitive Development Lab and Developmental Psychology Unit,
Faculty of Psychology, University of Warsaw, Warsaw, Poland

Abstract

Brain functions depend on cerebral transport mechanisms which are evidently propelled and regulated throughout the entire brain [1]. It is generally believed that the main driving force is the cardiac pulse [2] which, after arrival in the brain, travels effortlessly from the arterial into the veinous system seemingly leaving out what is in-between: namely the capillaries and the tissue, which both consist of a flow volume many magnitudes larger with a higher flow resistance than that of the blood vessels. If a pulsatile flow hits both the capillaries and the tissue [3], which are non-pulsatile regimes without vascular smooth musculature, then it should react like a small wave hitting a big inert mass. As a result, the wave should lose energy in a scattering process leading to damping, dispersion and reflection. However, the pulse exits the brain un-scattered [4] leaving us with the open question of what then drives cerebral dynamics. Here, we wanted to shed light on this mystery by studying microscopic parameters of cerebral dynamics. As such, we aimed to observe variations in Landau's order parameter [5] which may be accessible via multiple spin echos (MSE) [6]. We found MSE oscillations which appeared in brain tissue simultaneously with the arterial pulse. Those oscillations showed remarkable time pattern which revealed the spontaneous character of the underlying physiological mechanism. Our finding can be interpreted as a spontaneous symmetry breaking of the order parameter [7]; a phenomenon also occurring in superfluids. Superfluidity in cerebral dynamics has been recently discussed [8] as a possible answer to what may drive cerebral flow. It would give an eloquent explanation for the still controversially discussed cerebral autoregulation [9] because in superfluidity, heat would drive the flow [10] and not the cardiac pulse. Furthermore, a superfluid would flow dispersion-free whereby membranes would be of no obstacle because superfluids leak through every pore [11, 12].

In Nuclear magnetic resonance (NMR), two radio-frequency (RF) pulses combined with a magnetic field gradient are sufficient to generate multiple spin echos (MSE) as shown in solid Helium in [6], superfluid Helium [13] and in water [14]. In solid Helium and water, multiple echos are considered a result of an asymmetry in the non-linear demagnetisation field. This asymmetry can be introduced or amplified by gradient fields [6, 14, 15], RF pulses [16], and local field inhomogeneities and anisotropies [17, 18, 19, 20]. Signal intensity depends mainly on the asymmetry via the dipolar correlation distance at which the bulk of dipolar interactions become visible and on the effective spin size which depends mainly on the thermodynamical phase via the spin order [21]. MSE are characterised by the demagnetisation field's angle dependency which results in a signal cancellation at the so-called magic angle, distinguishing it from single spin echos (SSE). They have a common origin and contrast mechanism

*Corresponding author: christian@kerskens.me

bioRxiv preprint doi: https://doi.org/10.1101/219931; this version posted November 15, 2017. The copyright holder for this preprint (which was not certified by peer review) is the author/funder. All rights reserved. No reuse allowed without permission.

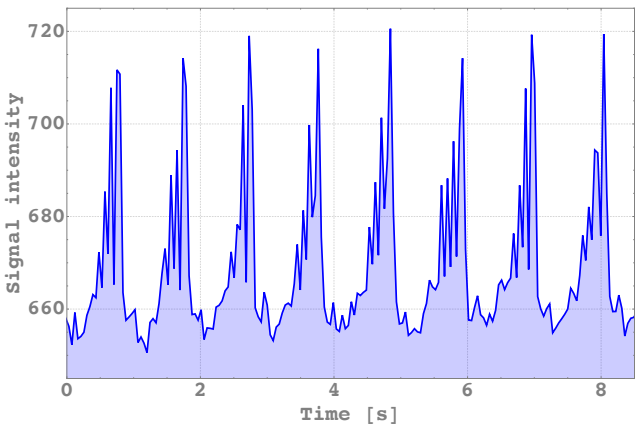

Figure 1: *Whole-slice averaged signal time course (selected by a mask) during 8 heart cycles. Subject had extra head fixation and was instructed to breath-hold during the period.*

[22, 23] with the intermolecular multiple quantum coherence (iMQC) which was introduced by Warren et al [15] in liquid NMR. MSE are present in many MRI sequences in particular in imaging series which are rapidly repeated. There, crusher gradients are added between two acquisitions with the primary intent to dephase any signal that remains from the previous excitation. This is where MSE come into the game. They appear where SSE disappears due to dephasing. In an imaging series with fast repetitions, single and multi spin echos will reach a steady state which then, in case of a human brain, will be disturbed by movement and physiological changes. In SSEs, possible signal alternations follow from the Bloch equations. They conclude changes of the magnetisation vector $\vec{M}_0$ which can be changed by brain movement, flow, and to some extent by diffusion and changes in T_1, T_2 and T_2^* relaxation. T_2^* fluctuations are mainly influenced by blood oxygenation and have become the subject of vibrant research with applications in psychology and medicine [24, 25]. Nevertheless, not much is known about how MSE may vary over time due to physiological fluctuations.

In our experiments, we used a conventional single-slice gradient-echo echo planar imaging series with a short repetition time (TR) instead of a dedicated MSE sequence as used in most studies. While this had some limitations towards the variability of some sequence parameters, it allowed a simultaneous acquisition of SSE and MSE which was important. When we used this sequence in healthy volunteers during rest, we found a predominate alternation with the cardiac frequency. In each cardiac cycle, we observed an interval which varied in length between 150 to 420ms showing a pattern as plotted in Figure 1. It was characterised by a signal increase of up to 15% which was modulated by an alternating zigzag. The start of the interval depended strongly on the head's mobility/fixation. The pattern as shown in Figure 1 was achieved using additional cushions inside the coil and by breath-holding (without taking a deep breath). Under normal condition, the zigzags usually only contain two maxima as shown in Figure 2.

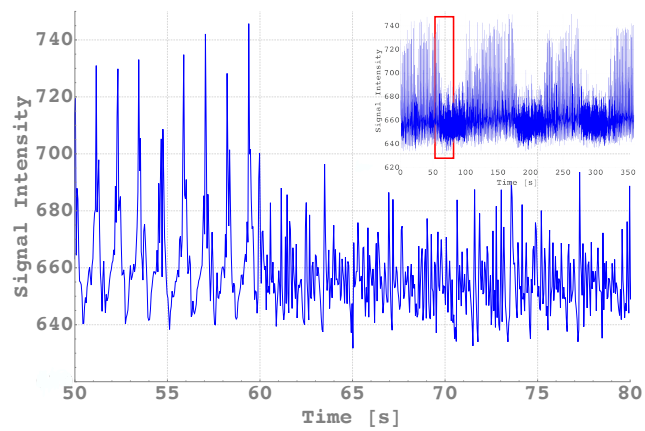

Figure 2: *Whole-slice averaged signal time course during normal breathing first. At 60s, the subject was instructed to hyperventilate. The inlet shows the total time course with 3 hyperventilation periods and the selected time interval in red.*

Figure 2 shows also how the signal changes with additional movement through hyperventilation. At 60s, the subject was instructed to hyperventilate with the result that the pattern immediately disappeared. In contrast to the initial variability, the end of the pattern was always well

bioRxiv preprint doi: https://doi.org/10.1101/219931; this version posted November 15, 2017. The copyright holder for this preprint (which was not certified by peer review) is the author/funder. All rights reserved. No reuse allowed without permission.

defined by an abrupt sudden annihilation which was coincident with the end-phase of the arterial pulse as shown in Figure 3A and the rise of veinous outflow as demonstrated in Figure 3B.

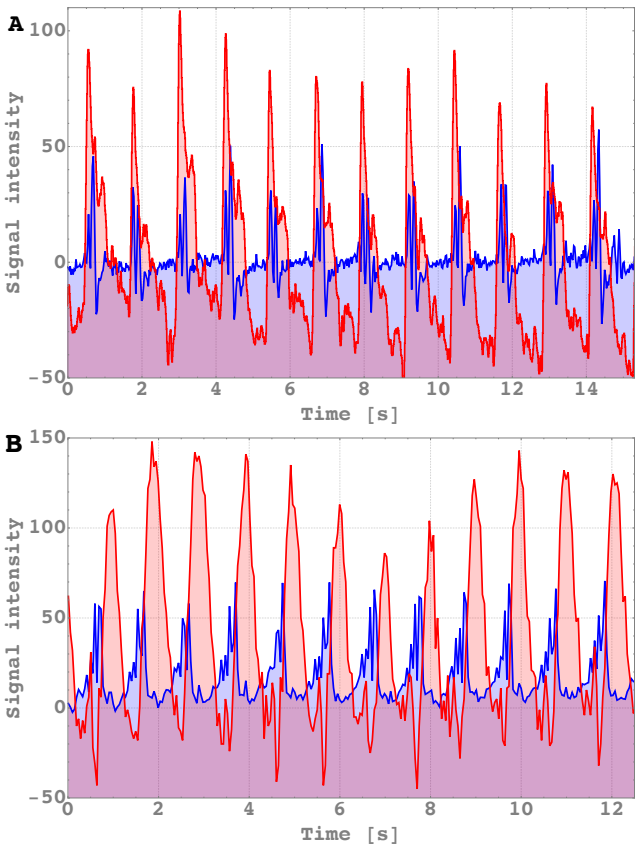

Figure 3: *Signal time course (Blue) during 12 heart cycles compared with **A**: Simultaneous oximeter reading of a finger (Red) and **B**: Signal time course (Red) of a vein.*

We located the pattern in tissue over the entire brain except in areas which are known to be prone to motion like the periventricular area [26]. We also found that the zigzag pattern, including the sudden end, could be restored while being averaged over the whole imaging slice (Figure 1). We used the averaged signal to investigate the contrast mechanism behind the signal pattern through varying the following sequence parameters: (a) the slice angulation, (b) the off-resonance frequency of the saturation pulses, (c) the flip angle (FA) with saturation pulses, and (d) the flip angle (FA) without saturation pulses. For (a), we found the angle dependency of the demagnetisation field $\sim (3 \cdot cos^2[\varphi - \Delta\theta] - 1)$ as shown in Figure 4 where φ was the a angle between the slice gradient and the main magnet field and $\Delta\theta = 9.25°$ a shift. The shift $\Delta\theta$ incorporated the mismatch between φ, and the angle between the asymmetry axis and the main magnet field θ which depended predominantly on the slice gradients, but also on the phase and readout gradient. For (b), we found a typical magnetisation transfer contrast (MTC) change for the baseline signal which depends on the off-resonance frequency (Figure 5A). In contrast, the peak intensity showed no significant changes in the same frequency range (Figure 5B).

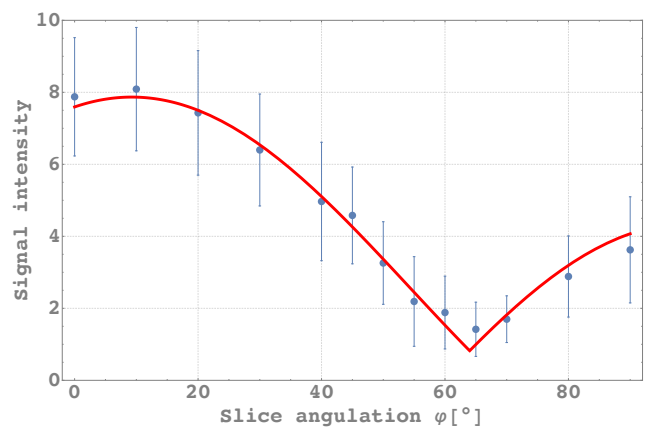

Figure 4: *Signal intensity plotted against the slice gradient angulation φ in respect to the magnetic main field.*

For (c), we found a maximum peak intensity at 45° (Figure 6). It followed the predicted signal course [27] in a range from 20 to 60°. For (d), we could extend our observation to 90° where we found a flat plateau following an initial signal increase. In comparison with (c) the signal was lower from 25° onwards. From our results, we conclude that the observed oscillation is generated by (a) two RF pulses which produced the zigzag pattern and (b) by the demagnetisation field which resulted in the angle dependency in Figure 4. They are the essential ingredients for

bioRxiv preprint doi: https://doi.org/10.1101/219931; this version posted November 15, 2017. The copyright holder for this preprint (which was not certified by peer review) is the author/funder. All rights reserved. No reuse allowed without permission.

MSE. At the magic angle, the cardiac pattern disappeared completely which leads us to conclude that it has no SSE component. With the exclusion of the linear part of the Bloch equation as a source of the signal pattern, we can now consider what could have possible impact on the non-linear part.

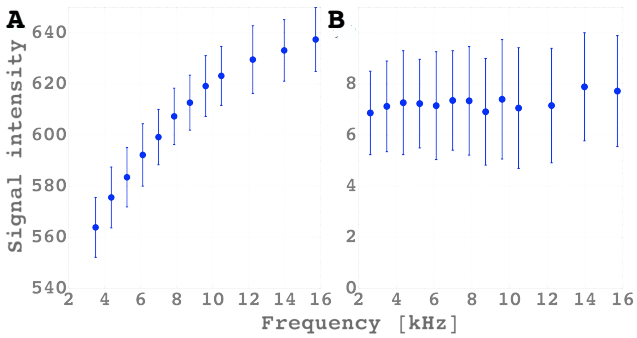

Figure 5: *Signal intensity plotted against the frequency offset of the saturation slices.* ***A****: averaged baseline signal.* ***B****: averaged signal of cardiac pattern*

At a 45° flip angle (for the case with saturation), where the pattern has a local maximum, we found that the signal is remarkably immune to MTC. The lack of MTC, which is a intramolecular mechanism, indicates that the observed MSE signal is not based on intramolecular multiple quantum coherences. In contrast, iMQC show a MTR dependency related to the rank of the tensors l that constituted the iMQC which is given as $(M_z/M_0)^l$ where M_z is the longitudinal magnetisation and M_0 its equilibrium value [28]. Our results indicate a zero rank for the case with the saturation pulses. From the zero rank and the optimum angle at 45° [27], we conclude here that the underlying mechanism is an intermolecular zero-quantum coherence (iZQC). Although, our result shows a clear iZQC contrast the physiological change is not specific to iZQC. This can be concluded from the flip angle dependency without the saturation pulses. There, we found in contrast to the exclusive iZQC with the saturation pulses, a mixture of all quantum orders n with maxima ranging from 45° (n=0), 60° (n=-2), 71° (n=-3), 75° (n=-4), 78.5° (n=-5), etc [27]. The lower signal intensity from 30° onwards resulted from destructive coherences of the multiple orders which were generated with different phases [21] and a rotation of the asymmetry axis due to the missing gradients of the saturation pulses.

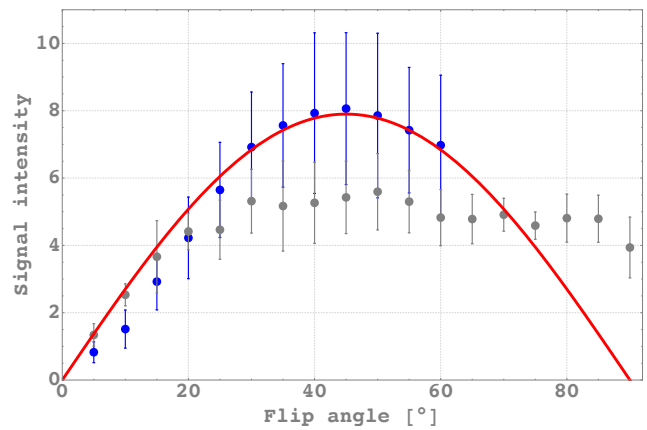

Figure 6: *Whole-slice averaged signal time course plotted against flip angle variation with saturation pulses (Blue) and without (Grey). IZQC prediction plotted in Red.*

We can now conclude that only changes in (a) structure [17, 18, 19, 20], (b) the long distance correlation [6, 18], or (c) the spin size number [15, 21] are possible to explain our observed signal. We exclude (a) because structural changes involving cell deformation, swelling or orientation on a time scale of some tens of milliseconds all over the brain would have an impact on total brain volume or pressure. Such a phenomenon is unknown and impossible to overlook.

For (b), we can compare the result between sequences with and without saturation again. The correlation distance defined by the crusher gradients is in the range 800 microns without saturation pulses and 140 microns with the saturation pulses. Both methods show only a marginal difference in the pattern signal intensity from which we can can conclude that we observed a strong long distance coupling with $\sim r^3$ (with r the distance between spins). It also

bioRxiv preprint doi: https://doi.org/10.1101/219931; this version posted November 15, 2017. The copyright holder for this preprint (which was not certified by peer review) is the author/funder. All rights reserved. No reuse allowed without permission.

means that (c) the spin size number increased during the pulsation.

In summary, we found evidence that during the pulse the brain switches into a system of higher ordering reflecting a thermodynamical phase transition. A sudden change in phase, as observed here, with a fast on- and offset bears all the hallmarks of spontaneous symmetry breaking [7]. Further discussions can be found in [8].

Materials and methods

40 subjects (between 18 and 46 years old) were scanned in a 3.0 T Philips whole-body MRI scanner (Philips, The Netherlands) operating with a 32-channel array receiver coil. Imaging protocols using standard single-shot GE EPI sequence were approved by the Trinity College School of Medicine Research Ethics Committee.
Initial experiments were carried out to establish a protocol that could deliver stable cardiac related signals over a range of subjects. The finalised parameters of the EPI sequence were as follows: FA = 45°, TR = 45 ms and the TE = 5 ms with a voxel size was 3.5 x 3.5 x 3.5 mm, matrix size was 64x64, SENSE factor 3, bandwidth readout direction was 2148 Hz, saturation pulse was 6 ms with 21mT/m gradient strength. The imaging slice was set coronal above the ventricle. In addition, two saturation slices of 5 mm (15mm above and 20mm below) in thickness were placed parallel to the imaged slice. These slabs were applied to suppress unwanted flow from blood vessels and mainly to introduce MTC. The following alternation (each with 1000 repetitions in five participants) were carried out, (a) slice angulation starting from coronal 0° to axial 90° in the steps as [0, 10, 20, 30, 40, 45, 50, 55, 60, 65, 70, 80, 90] , (b) the distance of the REST slabs were varied between 0.8 mm and 50 mm to alter the off-resonance frequency. The off-resonance frequencies were [2.62, 3.49, 4.36, 5.23, 6.11, 6.98, 7.84, 8.73, 9.60, 10.47, 12.22, 13.96, 15.71, 17.45] kHz, (c) Flip angle was varied for the case with saturation pulses from 5° to 60° in steps of 5° (60° was the power limit by the specific absorption rate (SAR)) and without saturation pulses from 5° to 90° in steps of 5°, (d) 9 slices were acquired at different positions, with each slice matching from bottom to the top the position of those acquired in the anatomical scan.
In four participants, we examined the motion sensitivity where we fixated the head with multiple cushions. During indicated intervals the subjects were asked to stop breathing for 20 s or to hyperventilate for 40 s. Finally, anatomical MRI images in all studies included a high-resolution sagittal, T1-weighted MP-RAGE (TR = 2.1 s, TE = 3.93 ms, flip angle = 7°).
Data processing was processed with Matlab 2014a (http://www.mathworks.co.uk/). Rescaling was applied to all datasets before any analysis using the MR vendor's instructions. Average time series were visually inspected in search for irregularities which were manually removed from the analysis leaving the rest of the time series unaltered. Manual segmentation was used to create a mask to remove cerebral spinal fluid (CSF) contributions. The first 100 scans were removed to avoid signal saturation effects. The manual segmentation of the masks was eroded to avoid partial volume effects at the edges.
The cardiac signal and baseline detection was based on the method proposed in Gomes and Pereira [29]. Final data presentation was carried with Mathematica (Wolfram Research, Champaign, Illinois).

Contributions

C.K. and D.L.P. discovered the phenomenon, experimentally, D.L.P. analysed the data, C.K. proposed the experiments and wrote the paper.

Acknowledgement

We would like to thank S. Joseph for carrying out the imaging protocols in our participants, R.Fallon for reading the manuscript, and Science Foundation Ireland for supporting D.L.P. from 2011-2015 (SFI-11/RFP.1/NES/3051).

bioRxiv preprint doi: https://doi.org/10.1101/219931; this version posted November 15, 2017. The copyright holder for this preprint (which was not certified by peer review) is the author/funder. All rights reserved. No reuse allowed without permission.

References

[1] Lassen, N. A. Cerebral blood flow and oxygen consumption in man. *Physiological Reviews* **39**, 183–238 (1959).

[2] Wagshul, M. E., Eide, P. K. & Madsen, J. R. The pulsating brain: A review of experimental and clinical studies of intracranial pulsatility. *Fluids and Barriers of the CNS* **8**, 5 (2011).

[3] Nedergaard, M. Garbage truck of the brain. *Science* **340**, 1529–1530 (2013).

[4] Iliff, J. J. *et al.* Cerebral arterial pulsation drives paravascular csf–interstitial fluid exchange in the murine brain. *The Journal of Neuroscience* **33**, 18190–18199 (2013).

[5] Landau, L. The theory of phase transitions. *Zh. Eksp. Teor. Fiz.* **7** (1937).

[6] Deville, G., Bernier, M. & Delrieux, J. M. NMR multiple echoes observed in solid ^{3}He. *Physical Review B* (1979).

[7] Anderson, P. W. More is different. *Science* **177** (1972).

[8] Kerskens, C. Superfluidity in biology. *in preparation* (2017).

[9] Ainslie, P. N. & Brassard, P. Why is the neural control of cerebral autoregulation so controversial? *F1000Prime Rep* **6:14** (2014).

[10] Ginzburg, V. L. & Sobyanin, A. A. Use of second sound to investigate the inhomogeneous density distribution of the superfluid part of Helium II near the lambda point. *JETP Lett. (USSR) (Engl. Transl.* **17**, 483–485 (1973).

[11] Kapitza, P. Viscosity of liquid helium below the λ-point. *Nature* **141**, 74 EP – (1938).

[12] Allen, J. F. & Misener, A. D. Flow of Liquid Helium II. *Nature* **141**, 75 (1938).

[13] Eska, G., Willers, H. G., Amend, B. & Wiedemann, C. Spin echo experiments in superfluid ^{3}He. *Physica B+ C* (1981).

[14] Bowtell, R., Bowley, R. & Glover, P. Multiple spin echoes in liquids in a high magnetic field. *Journal of Magnetic Resonance (1969)* **88**, 643 – 651 (1990).

[15] Warren, W., Richter, W. & Andreotti, A. Generation of impossible cross-peaks between bulk water and biomolecules in solution nmr (1993).

[16] Jerschow, A. Multiple echoes initiated by a single radio frequency pulse in NMR. *Chemical Physics Letters* **296**, 466–470 (1998).

[17] Bouchard, L., Rizi, R. & Warren, W. Magnetization structure contrast based on intermolecular multiple-quantum coherences. *Magn Reson Med* **48**, 973–979 (2002).

[18] Bowtell, R., Gutteridge, S. & Ramanathan, C. Imaging the long-range dipolar field in structured liquid state samples. *Journal of Magnetic Resonance* **150**, 147–155 (2001).

[19] Capuani, S., Alesiani, M., Branca, R. T. & Maraviglia, B. New openings for porous systems research from intermolecular double-quantum nmr. *Solid State Nuclear Magnetic Resonance* **25**, 153–159 (2004).

[20] Bouchard, L.-S., Wehrli, F. W., Chin, C.-L. & W., W. S. Structural anisotropy and internal magnetic fields in trabecular bone: Coupling solution and solid dipolar interactions. *Journal of Magnetic Resonance* **176**, 27–36 (2005).

[21] Baum, J., Munowitz, M., N., G. A. & Pines, A. Multiple-quantum dynamics in solid state NMR. *J. Chem. Phys. 83, 2015 (1985)* (1985).

[22] Jeener, J. Equivalence between the "classical"and the "Warren"approaches for the effects of long range dipolar couplings in liquid nuclear magnetic resonance. *The Journal of Chemical Physics* **112**, 5091–5094 (2000).

[23] Minot, E. D., Callaghan, P. T. & Kaplan, N. Multiple echoes, multiple quantum coherence, and the dipolar field: Demonstrating the significance of higher order terms in the equilibrium density matrix. *Journal of Magnetic Resonance* **140**, 200–205 (1999).

[24] Biswal, B., Zerrin Yetkin, F., Haughton, V. M. & Hyde, J. S. Functional connectivity in the motor cortex of resting human brain using echo-planar mri. *Magnetic Resonance in Medicine* **34**, 537–541 (1995).

bioRxiv preprint doi: https://doi.org/10.1101/219931; this version posted November 15, 2017. The copyright holder for this preprint (which was not certified by peer review) is the author/funder. All rights reserved. No reuse allowed without permission.

[25] Lee, M. H., Smyser, C. D. & Shimony, J. S. Resting-state fmri: A review of methods and clinical applications. *American Journal of Neuroradiology* **34**, 1866–1872 (2013).

[26] Nunes, R., Jezzard, P. & Clare, S. Investigations on the efficiency of cardiac-gated methods for the acquisition of diffusion-weighted images. *J Magn Reson* **177**, 102–110 (2005).

[27] Chen, Z., Zheng, S. & Zhong, J. Optimal rf flip angles for multiple spin-echoes and imqcs of different orders with the crazed pulse sequence. *Chemical physics letters* (2001).

[28] Eliav, U. & Navon, G. Enhancement of magnetization transfer effects by inter-molecular multiple quantum filtered NMR (2008).

[29] Gomes, E. F., Jorge, A. M. & Azevedo, P. J. Classifying heart sounds using multiresolution time series motifs: An exploratory study. In *Proceedings of the International C* Conference on Computer Science and Software Engineering*, C3S2E '13, 23–30 (ACM, New York, NY, USA, 2013).